Typical Complete Stress-Strain Curves of Coal

Khaled Morsy, Graduate Research Assistant
Syd S. Peng, Chairman and Charles T. Holland Professor
Department of Mining Engineering
West Virginia University
Morgantown, WV

Abstract

This study presents a typical stress-strain model for coal material using the available in-situ and laboratory tests data conducted on coal. This model can be used as a basic coal model in finite element applications. The effects of pillar width-to-height ratio and the confining pressure have been considered in this model. The extended Drucker-Prager model with mobilized friction angle was found to be very successful in simulating the proposed model.

Introduction

In recent years, due to the advancement of computer technology, especially in PC computers in the areas of memory capacity, speed, and cost, numerical modeling has been employed more frequently to solve the ground control problems in coal mining operations with encouraging results. Coal mining is a large dynamic event because it is a large-scale 3-D structure and moving constantly. In order to model this type of event with any degree of realistic sense, the 3-D numerical modeling must be used. In addition the geological conditions in most cases change constantly in three-dimensional way.

It is well known that the results of computer modeling cannot be any better than the accuracy of the input parameters. This includes the constitutive equations of the model materials (coal and rocks) and the variations of geological conditions.

With regard to the constitutive equation for coal, it has long been recognized that due to non-uniform stress distribution in the 3-D coal mine structures, some parts of those are subjected to yielding while other parts are still in the elastic range. Consequently, in order to model these structures with confidence, the complete stress-strain relationship of the model materials (rock and coal) must be considered.

This paper attempts to define a typical complete stress-strain relationship for coal based on literature research and the authors' experience in modeling and rock/coal property research in the past.

Typical constitutive model for coal

Are there typical complete stress-strain relationships for coal? In an attempt to identify the typical complete stress-strain relationships for coal, a detailed analysis for the available in-situ and laboratory tests data were conducted. The complete deformation characteristics of coal pillar can be described by the modulus of elasticity, strength and post-peak modulus. In addition, the complete stress-strain curves are highly dependent on the width-to-height ratio of the test specimens and the confining pressure.

Wagner (1974) conducted the first comprehensive in-situ tests of coal in South African coalfield. The tested pillars ranged from 1.968 ft to 6.56 ft wide with width-to-height ratio from 0.6 to 2.2.

Van Heerden (1975) conducted similar in-situ tests of coal pillars in South African coalfield. Pillars with cross-section of 4.592 ft square and width-to-height ratio from 1.14 to 3.39 were tested.

Das (1986) conducted a series of uniaxial compression tests on six Indian coal seams using a servo-controlled testing machine. Cylindrical specimens of 2.13 inches in diameter and width-to-height ratio from 0.5 to 13.5 were tested.

Medhurst and Brown (1998) conducted a series of triaxial compression tests on three Australian coal seams. Cylindrical specimens of 2.40, 3.98, 5.75 and 11.81 inches in diameter were tested under confining pressures from 0 to 1450 psi.

Modulus of Elasticity

From in-situ measurements, the modulus of elasticity was found to be a true material property and independent of the geometrical dimensions of the pillar such as size, height, and width-to-height ratio (Figure 1). Its average value was on the order of 5.8×10^5 psi. (Wagner, 1974; Van Heerden, 1975).

The same conclusion was reached from laboratory tests; the modulus of elasticity of the specimen is not influenced by its width-to-height ratio. The values between 3.5×10^5 and 8×10^5 psi were measured for different Indian coal seams (Das, 1986).

The modulus of elasticity for laboratory specimens shows no clear dependence on confining pressure either (Figure 2). The values between 3.16×10^5 and 6.2×10^5 psi were measured for different Australian coal seams by Medhurst and Brown (1998).

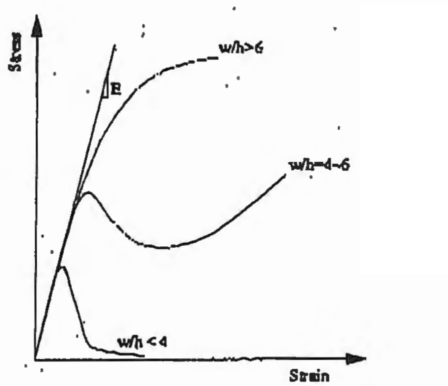

Fig. 1 Typical stress-strain curves for coal material under different width-to-height ratios.

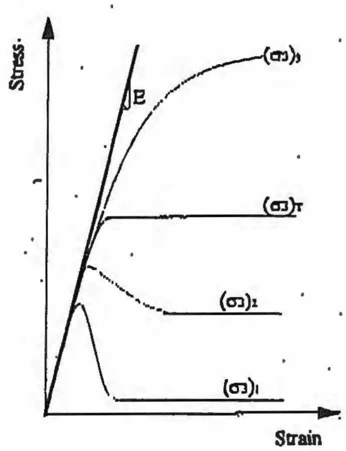

Fig. 2 Typical stress-strain curves for coal material under different confining pressures.

Post-Peak Behavior

At low width-to-height ratios, less than 3, the post-peak stresses within the pillar are continuously decreased as deformation increases and sometimes reaches zero (Figure 1). This happens because of lower triaxial confinement at the specimen center (Das, 1986; Wagner, 1974; Van Heerden, 1975).

In general, for specimens with width-to-height ratio greater than 4 or 6 the post-peak curves begins to fall initially followed by rising up to regain strength (Figure 1). This could be explained by the reconsolidation of the broken mass, which is due to high lateral constraints provided at the center of the specimen (Das, 1986).

Unlike the modulus of elasticity the width-to-height ratio has a marked effect on the post-peak modulus (i.e. maximum slope after strength failure) of coal pillars. Generally speaking, the post-peak modulus decreases with increasing width-to-height ratio (Figure 1). This indicates that the post-peak behavior of a pillar is a structural system property rather than an inherent material property.

Van Heerden (1975) concluded that the post-peak modulus reaches a constant value of 7.25×10^4 psi at a small width-to-height ratio of about 3. On the other hand Das (1986) concluded that the post-peak modulus become zero at higher width-to-height ratio of 10 and becomes positive with further increases in width-to-height ratio. Ozbay (1989) concluded that a pillar with width-to-height ratio of 5 has a zero post-peak modulus. Babcock and Bickel (1984) and Campoli et al., (1990) reported that even pillars with width-to-height ratio grater than 8 were subjected to bump failures. Pen and Barron (1994) fitted a large number of in-situ and laboratory data to determine the relationship between the width-to-height ratio and the normalized post peak modulus. Their relationship lies in the upper bound of the post-peak modulus of pillar estimated from the available data.
Barron (1992) shows that the post-peak modulus of coal specimen decreases with increase in confining pressure and becomes positive at high confining pressure (Figure 2).

Strength

To describe the complete stress-strain behavior of coal pillars, two types of strengths have to be defined, namely; peak strength and residual strength. The *peak strength* is defined by a stress value at which the slope of the stress-strain curve changes from the positive value to zero or negative value. The *residual strength* is defined by a stress level at which the slope of the stress-strain curve holds constant at approximately zero value while the pillar deforms.

According to the experience gained from the laboratory and in-situ experiments conducted on coal, the peak strength of large coal mass is lower than the peak strength determined by laboratory testing on small specimens. For South African coal, Bieniawski (1968) concluded that 5 ft cubic specimens constitute the critical size beyond which the peak strength of the coal block remains constant. Bieniawski (1992) estimated the critical size for US coal seams to be 36 in. Mark (1990) assumed an in-situ compressive strength of 900 psi for US coal fields.

Many researchers (Holland-Gady, 1957; Holland, 1964; Obert and Duvall, 1967; Salamon and Munro, 1967; Bieniawski, 1968; Wagner, 1974; Van Heerden, 1975; and Das, 1986) studied the effect of width-to-height ratio on the peak strength of coal pillars. Generally speaking, in spite of the form of the developed relationships between the width-to-height ratio and the peak strength, the peak strength increases with increasing width-to-height ratio (Figure 1).

Figure 3 shows the triaxial tests conducted on six coal seams, namely; Wabash seam No. 5 (C1), Blue Creek (C2), Mary Lee (C3), Pittsburgh seam (C4), Castlegate No. 3 (C5), and Castlegate No (C6). It is obvious that the coal peak strength is linearly proportional to the confining pressure (Sun and Peng, 1993). The correlation coefficients for different coal seams range from 0.79 to 0.99. The same conclusion could be drawn from the data published by Medhurst and Brown (1998).

Unlike the peak strength, only a few researchers have studied the effect of pillar width-to-height ratio and the confining pressure on the residual strength. From the data published by Das (1986), it could be concluded that the pillar residual strength is increased exponentially with increasing width-to-height ratio.

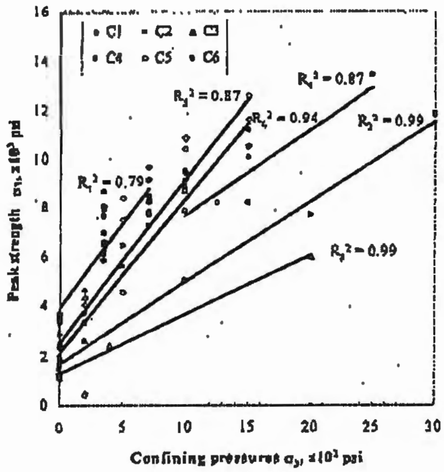

Fig. 3 Peak strength curves for coal samples of different coal seams.

Figure 4 shows the linear relationship between the coal residual strength and confining pressure after Medhurst and Brown (1998). Based on the analysis mentioned previously, the typical peak strength and residual strength curves for coal material are shown in Figure 5.

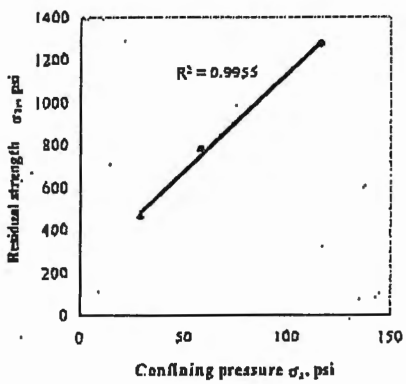

Fig.4 Residual strength curve for coal samples drawn after Medhurst and Brown (1998).

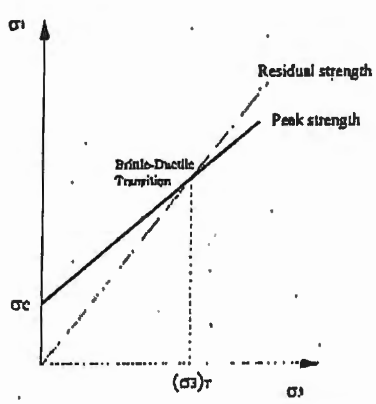

Fig.5 Typical peak strength and residual strength curves for coal material.

Brittle-Ductile Transition

It is well recognized that, the behavior of most rocks change from brittle to ductile at some elevated confining pressure (Figure 2). It is postulated that such failure can occur in coal in the range of confining pressure normally encountered in mining. The brittle-ductile transition point is defined by Barron (1992) as the point of intersection between the peak stress failure criterion and the residual strength criterion (Figure 5).

Mogi (1971) defined the residual strength criterion for many rocks as linear relationship between the residual strength, σ_{r1} and the confining pressure, σ_3:

$$\sigma_{r1} = 3.4\sigma_3 \quad \text{.......................................(1)}$$

Isotropic strain hardening-softening model for coal material

An elastic-plastic material model with no hardening has been used frequently in numerical modeling to simulate the behavior of coal pillars. However as explained above, the real stress-strain curve for coal exhibits both hardening and softening behavior depending on the state of stress.

The extended Drucker-Prager model, available in ABAQUS FE package (Hibbitt et al. 1998), describes the behavior of rock-like materials in which the yield behavior depends on the equivalent pressure stress. It allows a material to harden and/or soften isotropically.

Drucker-Prager Criterion

The classical Drucker-Prager yield condition, (Drucker and Prager, 1952) is expressed as follows: -

$$f \equiv \alpha J_1 + \sqrt{J_{2D}} - k = 0 \quad \text{..........................(2)}$$

where,

α and k = Material property constants related to cohesion and angle of internal friction;
J_1 = First invariant of stress tensor;
J_{2D} = Second invariant of the deviator stress tensor.

$$J_1 = \sigma_1 + \sigma_2 + \sigma_3 \quad \text{..................................(3)}$$

$$J_{2D} = \frac{1}{6}\left[(\sigma_1 - \sigma_2)^2 + (\sigma_2 - \sigma_3)^2 + (\sigma_1 - \sigma_3)^2\right] \quad \text{.......................(4)}$$

where

σ_1 = Major principal stress.
σ_2 = Intermediate principal stress.
σ_3 = Minor principal stress.

Equation 2 represents a straight line on a J_1 versus J_{2D} plot (Figure 6a). In the three-dimensional stress space, the criterion is expressed by a right circular cone, and the projection on the Π plane is a circle, as shown in (Figure 6b). Different material constants will produce different shapes of cones and circles. As shown in Figure 6, the intermediate circle represents the yield surface at peak strength of coal. Prior to yielding, all stress conditions inside that circle are in the elastic state. When the point representing the stress condition reaches the surface of the yield circle, the coal begins to yield.

Depending on the state of stress, with further plastic deformation the material may experience strain hardening and the yield surface expands outward. On the other hand, if the material falls in the range of strain softening, plastic deformation causes the yield surface to contract or move inward.

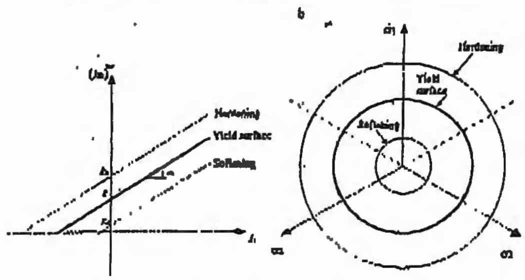

Fig.6 Linear Drucker-Prager criterion on
(a) the meridional plane;
(b) Π plane.

Generally, the hardening or softening behavior is achieved by making the parameter k dependent on a measure of plastic deformation (e.g. plastic volumetric change), while the other parameter α holds constant (Maier and Hueckel, 1979). So the Drucker-Prager criterion for isotropic hardening/softening can be rewritten as:

$$f \equiv \alpha J_1 + \sqrt{J_{2D}} - k^* = 0 \quad \text{..............................(5)}$$

where k^* is a mobilized cohesion parameter.

Making the parameter α constant makes the peak strength and the residual strength failure criteria parallel; i.e., the brittle-ductile transition is not possible and it leads to a constant post peak modulus at any confining pressure in triaxial tests. This result contradicts with coal behavior, as explained before.

Friction Hardening

To illustrate the friction hardening, consider the strain softening model in Figure 7. The deviator stress q increases in the early stage of loading until it reaches the peak strength and then decreases and finally reaches the residual strength. On the other hand, the frictional component increases during the whole deformation process up to and remain at residual strength state (Adachi et al., 1991). Adachi and Oka (1985) defined the rapid increase of frictional component during loading process as stress history tensor. The difference between applied stress and stress history tensor corresponds to the cohesive strength due to cementation or bonding. The cohesive strength can be destroyed by deformation.

To express the increase of the frictional component during material deformation, a strain-dependent quantity α^*, referred to as the mobilized angle of friction, will be used. The mobilized angle of friction gradually increases with strain to reach the limit angle of friction when the plastic strain has reached its constant value (Figure 7). Hansen (1965) developed many formulas expressing such behavior.

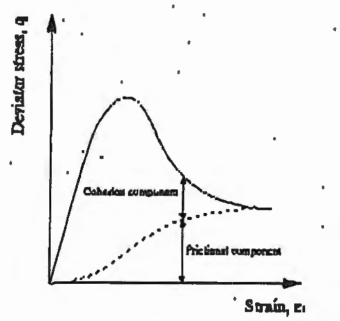

Fig. 7 Friction hardening vs. cohesion softening for coal material.

Introducing both of the mobilized cohesion k^* and the mobilized angle of friction α^*, the Drucker-Prager yield function can be expressed as:

$$f \equiv \alpha^* J_1 + \sqrt{J_{2D}} - k^* = 0 \quad \text{..............................(6)}$$

Triaxial test for coal material

Model Description

The model studies a simple triaxial test: an axisymmetric coal sample compressed between two smooth platens, one of which is held fixed and the other has prescribed vertical motion. The coal specimen is first loaded by constant pressure σ_3; 0, 200, 500, 1000, 1500, 2250, 3000, 4000, 5000 psi. Then the top platen is moved downward to compress the specimen. Figure 8 defines the model geometry.

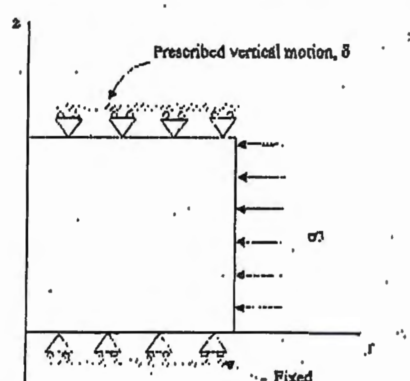

Fig.8 Triaxial compression test with smooth platens.

Based on the above study, a rectilinear stress-strain curve (Figure 9) has been proposed to simulate the in-situ compression test of coal material.

The typical Drucker-Prager parameters for coal material are given in Table 1. The coal residual strength is assumed to follow Mogi (1971) criterion given by Equation (1). So the residual friction angle α_r is estimated to be 53.13 degrees and the brittle-ductile transition confining pressure is 2250 psi.

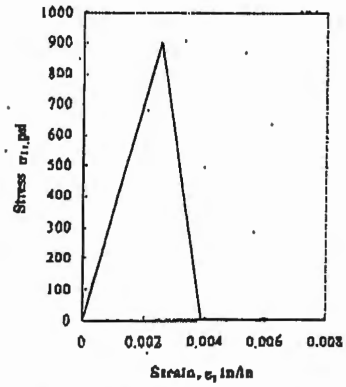

Fig.9 Rectilinear stress-strain curve for coal model used for the simulations.

Table 1 Typical coal properties used in FE models

Parameter	Value
Elastic modulus E, psi	$3.5*10^5$
Poisson's ratio ν	0.3
Peak strength σ_p, psi	900
Residual strength σ_r, psi	4.8
Post-peak modulus λ_m, psi	$7.0*10^5$
Initial friction angle α_i, degree	50.19
Residual Friction angle α_r, degree	53.13

For the sake of simplicity, the friction hardening is simulated by linearly increasing the friction angle with respect to the equivalent plastic strain. On the other hand the cohesion softening is obtained by linearly reducing the cohesion with respect to the equivalent plastic strain (Figure 10).

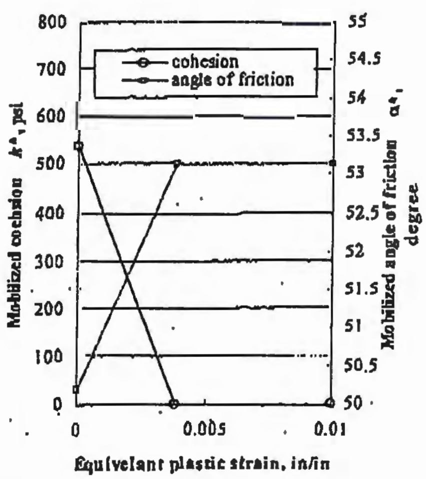

Fig. 10 Strain softening parameters used for the simulations.

Results and Discussion

To illustrate the importance of mobilizing the angle of friction in the Drucker-Prager model, two types of FE models are conducted subjected to the same boundary conditions. The first type represents the Drucker-Prager model with constant friction angle of 50.19 degrees while the second type represents the Drucker-Prager model with mobilized angle of friction.

Figure 11a shows the estimated deviator stress-strain curves of coal specimen under different confining pressures using the Drucker-Prager model with constant angle of friction. It is obvious that this model doesn't satisfy two important characteristics of typical coal model. First, the post-peak modulus is observed to be independent of the confining pressure. Second, the model doesn't show a transition from brittle to ductile behavior even at a high confining pressure of 5000 psi.

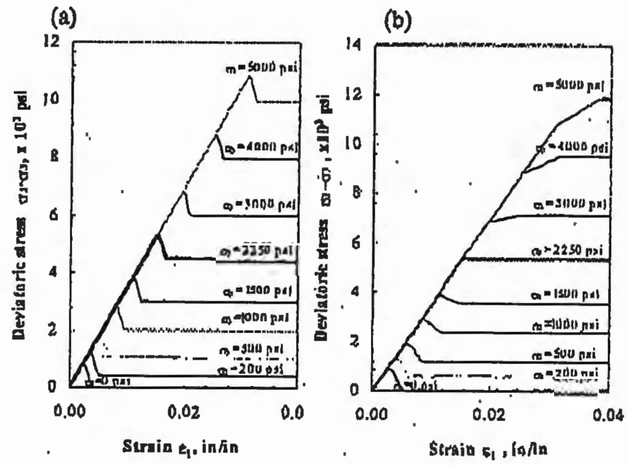

Fig. 11 Simulation results of triaxial tests for Drucker-Prager model with

a. Constant angle of friction.
b. Mobilized angle of friction

On the other hand, Figure 11b shows the estimated deviator stress-stain curves of coal specimen under different confining pressures using Drucker-Prager model with mobilized angle of friction. Figure 12 shows that this model was able to show both the hardening and softening behaviors of coal specimen under different confining pressures.

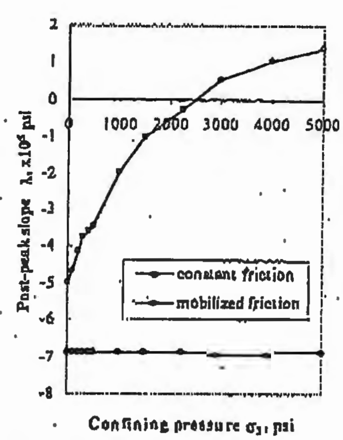

Fig. 12 Estimated Post-peak modulus vs. applied confining pressures.

Since the effect of friction angle mobilization starts once the specimen begins to yield, there are no differences between the peak strengths predicted by both types of Drucker-Prager model (Figure 13). On the other hand, Figure 14 shows that the differences between the residual strengths predicted by the Drucker-Prager models increases with increasing confining pressure.

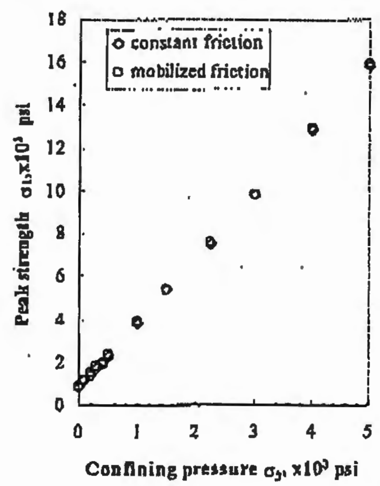

Fig. 13 Estimated peak strength curves.

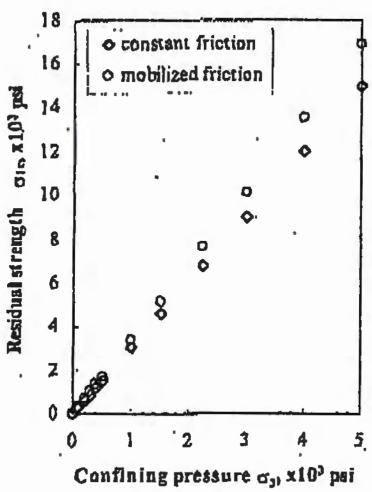

Fig. 14 Estimated residual strength curves.

Effect of specimen width-to-height ratio on its deformation characteristics

Model Description

The model is used to study the effect of specimen width-to-height ratio on its deformation characteristics using Drucker-Prager model with mobilized angle of friction. The same inputs defined in Table 1 have been used in this study. Axisymmetric coal samples of 2 inches diameter with different heights, 4, 6.16, 8, 10, 13.34, 16 and 20 inches, are compressed between two steel platens, one of which is held fixed and the other is moved according to the prescribed vertical motion. A friction angle of 14° has been assigned between the coal sample and the steel platens.

The specimen grid was generated with 0.05-inch square elements. The maximum loading rate during the test was .0004 inch/sec. Figure 15 defines the model geometry and boundary conditions.

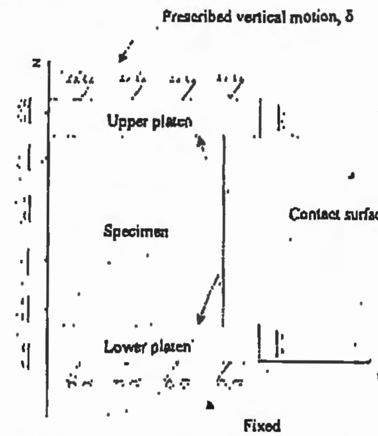

Fig. 15 Uniaxial compression test with regular platens.

Results and Discussion

Figure 16 shows the estimated stress-strain curves for coal specimens with different width-to-height ratios using the Drucker-Prager model with mobilized angle of friction. The model was able to show the independency of the Elastic modulus. The specimen's softening behavior was obvious at small width-to-height ratios, up to 4, while it shows a hardening behavior at high width-to-height ratio of 10. The model shows the reconsolidation behavior reported by Das (1986) at a width-to-height ratio of 6.67.

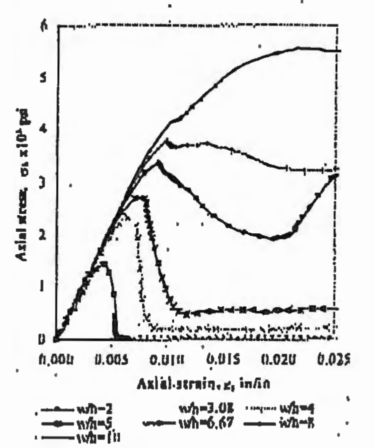

Fig.16 Estimated stress-strain curves at different width-to-height ratios.

The post-peak modulus (maximum slope after peak-strength) was calculated from the stress-strain curves and plotted against the width-to-height ratio as shown in Figure 17. The post-peak modulus is decreasing with increasing specimen width-to-height ratio and it becomes around zero at width-to-height ratio of 10.

Figure 18 shows the slow change of residual strength at low width-to-height ratio, less than 5, and the rapid change at higher width-to-height ratios. Also, it shows the strengthening effect of specimen width-to-height ratio, where the specimen peak strength increases with increasing specimen width-to-height ratio.

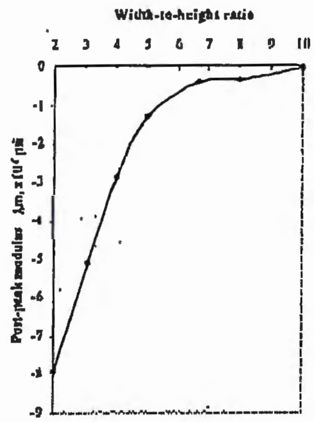

Fig. 17 Estimated Post-peak modulus vs. specimen width-to-height ratio.

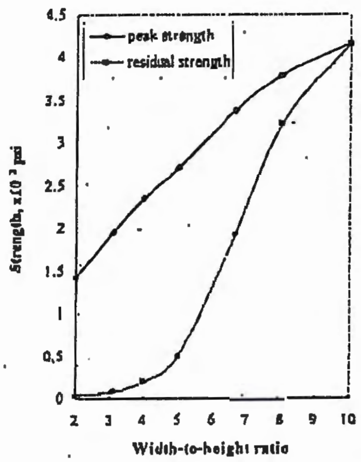

Fig. 18 Estimated peak and residual strength vs. specimen width-to-height ratio.

Conclusions

- A typical model for coal pillars, based on the in-situ and laboratory tests was proposed.
- The proposed model considers the effects of the width-to-height ratio and confining pressure on the deformation behaviors of coal pillar.
- The Drucker-Prager model with mobilized angle of friction was found very successful to simulate the proposed model.

References

1. Wagner, H., 1974, " Determination of the Complete Load-Deformation Characteristics of Coal Pillars," Proceedings of the 3rd International Congress on Rock Mechanics, ISRM, Denver, CO, pp. 1076-1081.
2. Heerden, W. L. V., 1975, "In Situ Complete Stress-Strain Characteristics of Large Coal Specimens," Journal of South African Institute of Mining and Metallurgy, March, pp. 202-217.
3. Das, M. D., 1986, "Influence of Width/Height Ratio on Post-Failure Behavior of Coal," International Journal of Mining and Geological Engineering, Vol. 4, pp. 79-87.
4. Medhurst, T. P. and Brown, E. T., 1998, " A Study of the Mechanical Behavior of Coal for Pillar Design," International Journal of Rock Mechanics and Mining Science, Vol. 35, No. 8, pp. 1087-1105.
5. Ozbay, M. U., 1989, "The Stability and Design of Yield Pillars Located at Shallow and Moderate Depths," Journal of South African Institute of Mining and Metallurgy, March, pp. 73-79.
6. Babcock, C. O. and Bickel, D. L., 1984, "Constraint – the Missing Variable in the Coal Burst Problem," Proceedings of the 25th U.S. Symposium on Rock Mechanics, pp. 639-647.
7. Campoli, A. A., Barton, T. M., Dyke, F. C. V., and Gauna, M., 1990, " Mitigating Destuctive Longwall Bumps through Conventional Gate Entry Design," RI 9325, U.S. Bureau of Mines.
8. Pen, Y. and Barron, K., 1994, "The Role of Local Mine Stiffness in Pillar Bump Prediction, " Proceedings of the 1st North American Rock Mechanics Symposium, University of Texas, Austin, pp. 1017-1025.
9. Barron, K., 1992, "A Revised Model for Coal Pillars," Proceedings of the Workshop on Coal Pillar Mechanics and Design, US Bureau of Mines, IC 9315, pp. 144-157.
10. Bieniawski, Z.T., 1968, "The Effect of Specimen Size on Compressive Strength of Coal," International Journal of Rock Mechanics and Mining Science, Vol. 5, pp. 325-535.
11. Bieniawski, Z.T., 1992, "A Method Revised: Coal Pillar Strength Formula Based on Field Investigations," Proceedings of the Workshop on Coal Pillar Mechanics and Design, US Bureau of Mines, IC 9315, pp. 158-165.
12. Mark, C., 1990, "Pillar Design Methods for Longwall Mining (ALPS)," US Bureau of Mines, IC 9247, pp. 1-53.
13. Holland, C. T., and Gaddy, F. L., 1957, "Some aspects of Permanent Support of Overburden on Coal Beds," Proceedings of West Virginia Coal Mining Institute, pp. 43-66.
14. Holland, C. T., 1964, " The Strength of Coal in Mine Pillars," Proceedings of the 6th Symposium on Rock Mechanics. University of MO, Rolla, Mo, pp. 450-466.
15. Obert, L. and Duvall, W. I., 1967, "Rock Mechanics and the Design of Structures in Rock," Wiley, New York, pp. 542-545.
16. Salamon, M. D. G., and Munro, A. H., 1967, "A Study of the Strength of Coal Pillars;" Journal of South African Institute of Mining and Metallurgy, Vol. 68, pp. 55-67.
17. Sun, G. C. and Peng, S. S., 1993, "Rock Mechanics Property

Data Bank for Coal Measure Strata," Proceedings of 12th International Conference on Ground Control in Mining, Morgantown, WV, pp. 330-341.

18. Mogi, K., 1971, "Fracture and Flow of Rocks Under High Triaxial Compression," Journal of Geophysical Research, Vol. 76, No. 5, pp. 1255-1269.
19. Hibbitt, D., Karlsoon, B., and Sorensen, P., "ABAQUS Manual" Version 5.8, Hibbitt, Karlsoon & Sorensen, Inc., 1998.
20. Drucker, D.C., and Prager, W., 1952 "Soil Mechanics and Plastic Analysis or Limit Design," Quart Applied Mathematics, Vol. 10, No. 2, pp. 157-165.
21. Maier, G. and Hueckel, T., 1979, "Nonassociated and Coupled Flow Rules of Elastoplasticity for Rock-Like Materials," International Journal of Rock Mechanics and Mining Science, Vol. 16, pp. 77-92.
22. Adachi, T., Zhang, F., Oka, F., and Yashima A., 1991, "Finite Element Analyses with Strain-Softening Constitutive Model," Computer Methods and Advances in Geomechanics, Beer, Booker & Carter (eds), pp. 535-540.
23. Adachi, T. and Oka, F., 1985, "An Elasto-Plastic Constituitive Equation of Geological Materials with Memory," Proceedings of the 5th ICNMIGNagoya, pp. 293-300.
24. Hansen, J. B., 1965, "Some stress-Strain Relationships for Soils," Proceedings of the 6th International Conference of Soil Mechanics and Foundation Engineering, Montreal, Vol. 1, pp. 231-234.